“The Polar Upper Atmosphere: from Science to Operational Issues”

Coronal Mass Ejection modelling and forecasting

(D. Del Moro)

CMEs are huge magnetic field flux ropes which erupts from the Sun's corona carrying away significant amounts (average mass is $2x10^{12}$ kg) of plasma. As they lift off from the solar atmosphere, they can accelerate up to >3000 km/s speeds, thus sweeping and compressing the slower solar wind, creating shock waves. In those shocks, energy exchange processes can accelerate particles up to GeV values, creating solar cosmic rays, better known as SEPs. CMEs are very often, but not always, associated to a flare event, signaling a large reconfiguration of the magnetic field on the solar surface and successive release of a filament of magnetized plasma. A CME hitting the terrestrial magnetosphere will induce disturbances of the magnetic field (magnetic storm) and can alter the environment in and within the radiation belts, with consequences on satellite and astronaut safety. The occurrence frequency of CMEs and any other solar activity is strongly modulated by the magnetic cycle. In fact, it is the Sun's magnetic field that serves as the energy source and dynamical engine of the solar explosive events.

In this lesson, I will provide an introduction on the processes at the base of CME ejection and a walk-through on the CME propagation models presently available.

What do we know about CMEs?

Angular width

Narrow: <10°

Jet-like

“Normal”: up to 360°

(halo CME)

Velocity and energy

v_PoS = 20-3500 km/s

E_kin = 10^22-10^25 J

Morphology and mass

Normal CME:

Average mass = 2x10^12 kg

Frontal loop = shock or arcade

Cavity = expansion

Bright Core = erupting filament

Association with flares and filament eruptions

w Flares: Often, but not always

w Filaments: Very strong

Occurrence rate

Depends on the cycle:

solar minimum: 1-2 x day

solar maximum: 6-8 x day

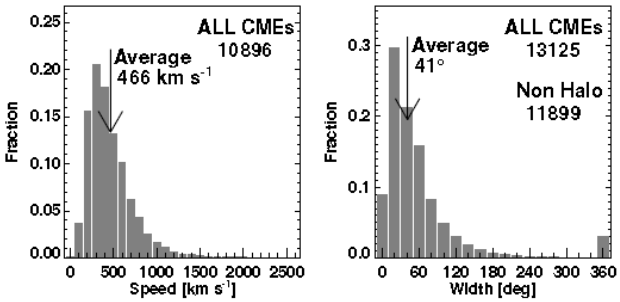

Illustration 1: Speed and width distributions of all CMEs from the CDAW database

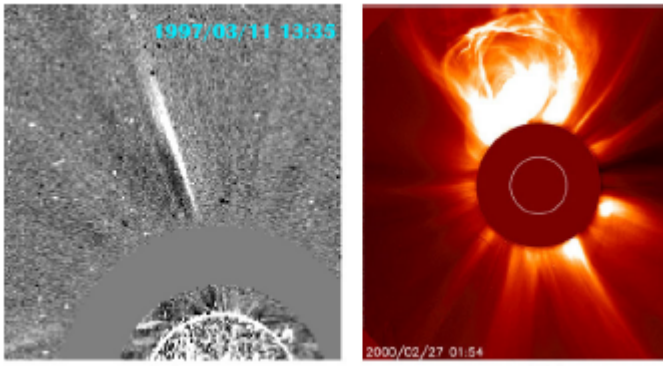

Illustration 2: White-light images of two types of typical CMEs (from SOHO/LASCO database). Left: A “narrow” CME on 1997 March 11, where the 195 ˚A disk image is overplotted on the occulting disk. Right: a “normal” CME on 2000 February 27 with a three-part structure, i.e., a frontal loop, a cavity, and a bright core. The white circle marks the solar limb.

What is the 'standard' model of a 'normal' CME?

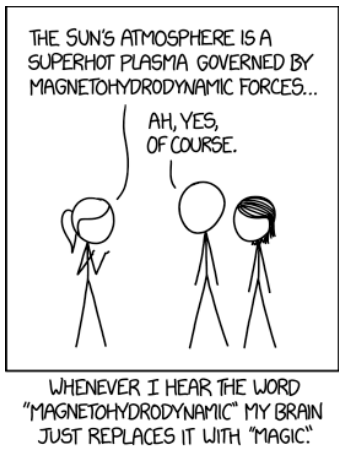

"*The CME is an erupting magnetic flux rope system*"

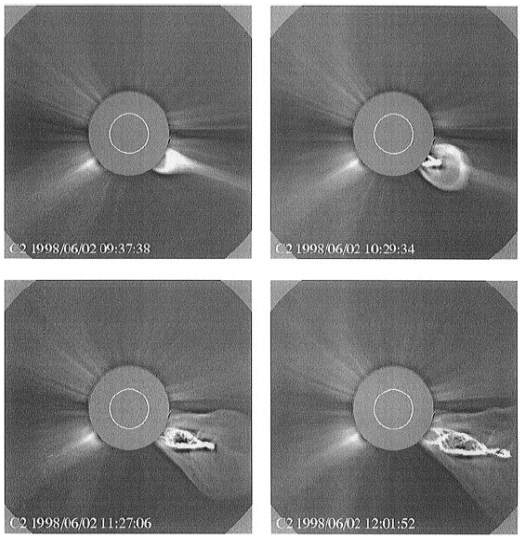

Illustration 3: Evolution of a "classic" CME observed by the LASCO C2 coronagraph.

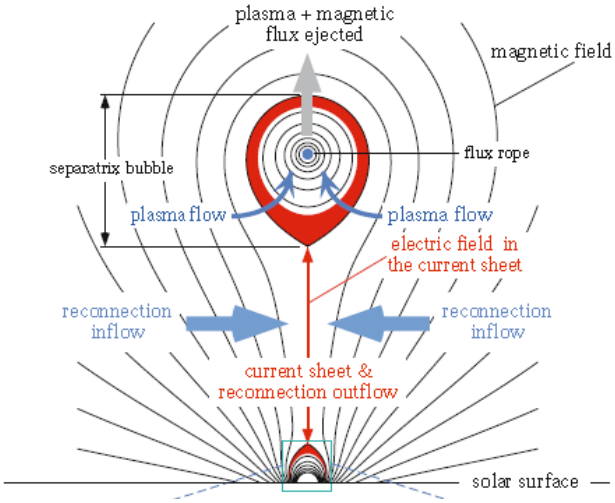

Illustration 4: Schematic diagram of the 'standard' CME model

- **Progenitor**
  Strongly twisted or sheared magnetic structure in a metastable equilibrium or close to a non-equilibrium state
- **Trigger**
  Tether-cutting or flux cancellation mechanism
  Shearing motions
  Instabilities
  Mass drainage
- **Acceleration and propagation**
  Solar wind
  instabilities
  re-connection in the current sheet
- **Bright core**
  Erupting filament

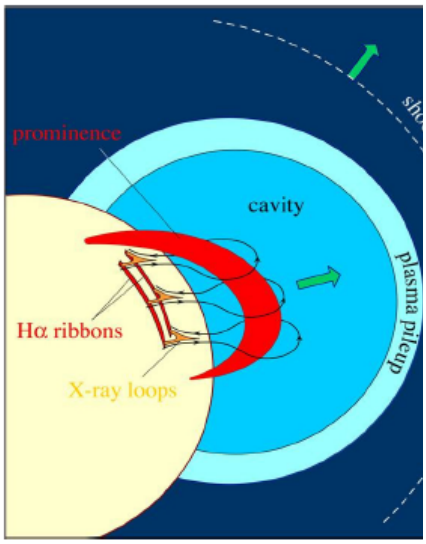

Illustration 5: Another point of view for the diagram of the 'standard' CME model .

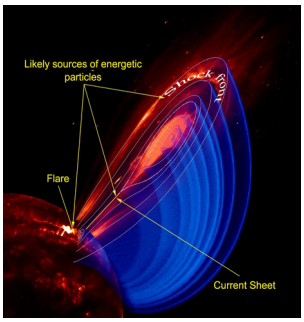

Illustration 6: Yet another point of view for the diagram of the 'standard' CME model .

- **Cavity**
  density is relatively low
  magnetic field line stretching pushed by the erupting flux rope
- **Frontal loop**
  part of the flux rope? Mass motion?
  plasma pileup
- **Lateral expansion**
  significant expansion only in the low corona
- **Shocks**
  piston-driven shock
  upward and downward at re-connection sites

DEBATES!!

- Magnetic re-connection: really needed?
  flares generally occur minutes after the CME is initiated
  → re-connection takes place after the CME progenitor is stretched up in the low corona
  CME may erupt via ideal MHD processes

- Are Fast CMEs different from slow CMEs?
  CMEs associated with flare vs CMEs associated with an erupting filament
  (Probably not) → which factors determine the CME velocity?
- Are Halo CME special?
  They are on average twice faster than normal CMEs!
  (Probably not)

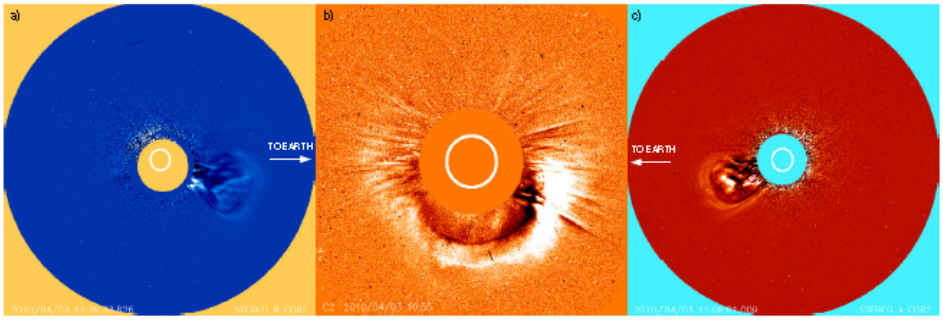

Illustration 7: Images of the same Earth-directed CME obtained from three different viewing locations within an hour: a) from STEREO/COR2-B on 3 April 2010 at 11:39 UT, b) from LASCO/C2 at 10:55 UT,and c) from STEREO/COR2-A on the same day at 11:08 UT. At this time (April 2010) the STEREO spacecraft were approximately 70° in longitude from the Sun-Earth line and ~ 140° from each other. The different appearances of this same CME observed at around the same time demonstrate the need to consider perspective in measuring CME properties.

- What is the real nature of the front loop?
  - a) fast-mode MHD waves excited by the pressure pulse
  - b) bundle of the background coronal magnetic field lines filled with plasma
  - c) twisted flux rope expanding and broadening
  - d) shock or compression wave from magnetic filed lines stretching

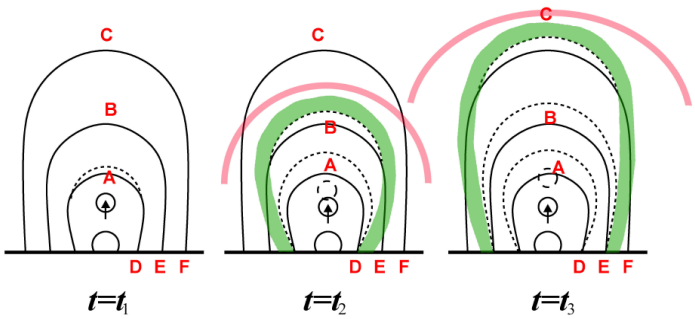

Illustration 8: A schematic sketch of the formation mechanism of CME leading loops, where the CME leading loop (green) are apparently-moving density enhanced structure that is generated by the successive stretching of magnetic field lines as the erupting core structure continues to push the overlying field lines to expand outward successively. The piston-driven shock is shown as pink lines

Which CME propagation models do we have? How do we forecast?

"After the launch", the CME is somewhat easier to model:

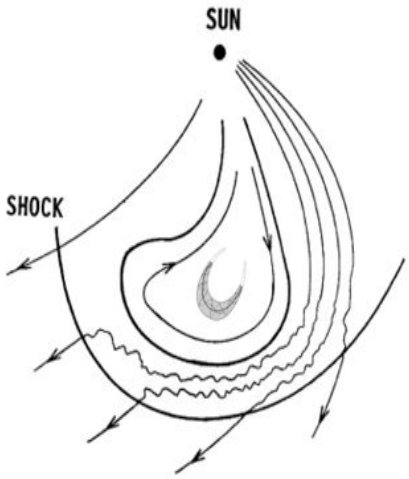

Illustration 9: In general an ICME has a complicated structure!

After the launch: >20 R_sun away

Negligible gravity

Negligible "acceleration"

MHD Drag against environment (solar wind)

A) MHD models → numerical simulations

ENLIL- based model

EUHFORIA model

SUSANOO-CME model

… there are others!

B) HD models → analytic solutions

Drag Based Model

- PDBM

- DBEM

… there are others, too!

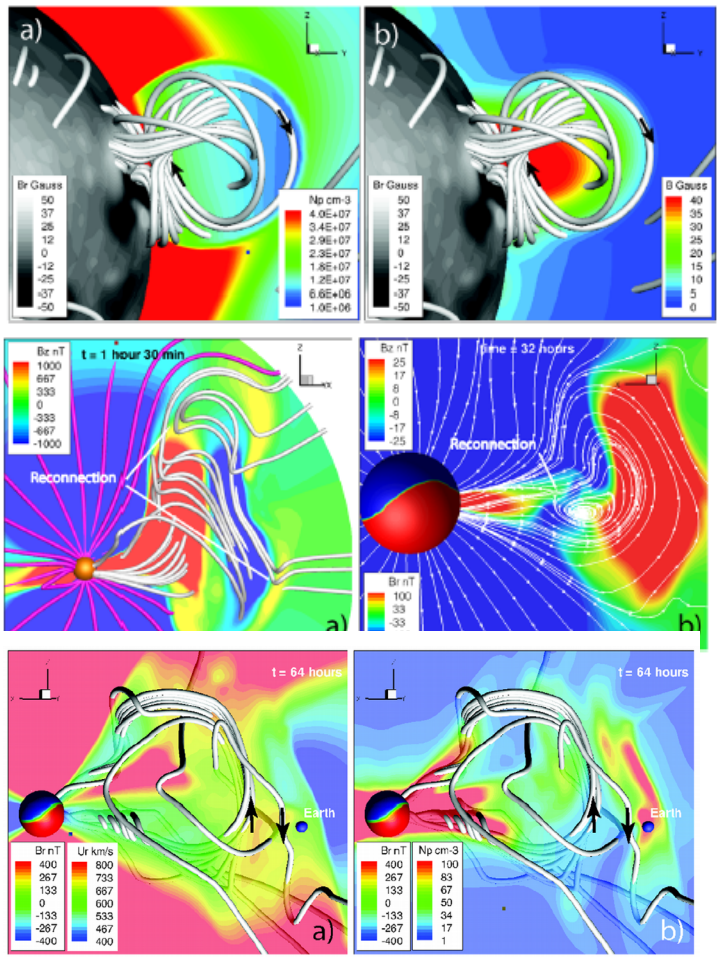

Illustration 10: Top: flux rope inserted in the solar corona; left: proton density, right: magnetic field strength. Middle: as the flux rope propagates, its magnetic field reconnects with the IMF; re-connnection events at 90 min (left) and 32 h (right). Bottom: the structure of the CME 64 h after initiation: the CME-driven shock has passed the Earth; left: radial velocity, right: proton density.

WSA-ENLIL + (CONE) model

WSA-ENLIL is a global 3D MHD model which provides a time-dependent description of the background solar wind plasma and magnetic field into which a spherical or ellipsoid shaped CME can be inserted.

A CME-like hydrodynamic structure is launched into the solar wind and magnetic field computed from the WSA coronal model at 21.5 Rs.

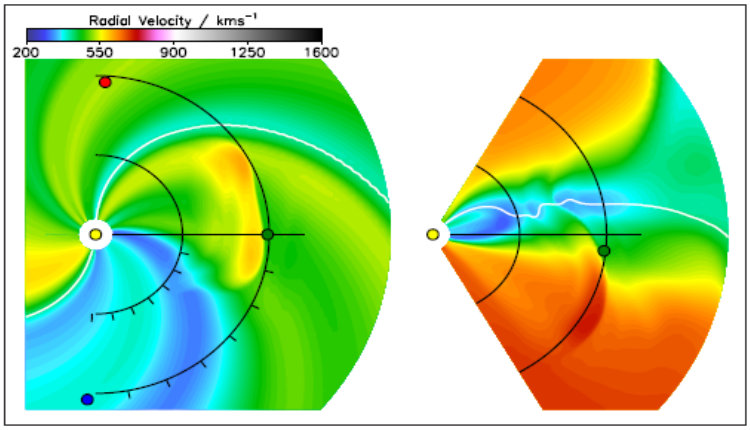

Illustration 11: Sample output for WSA–Enlil cone run for the 15 February 2011 multiple coronal mass ejection (CME) event. Graphic shows the velocity structure for three CMEs in the outburst at the time the largest CME was predicted to reach Earth, about 1500 UTC on 17 February. Image at left depicts the velocity structure in the ecliptic plane, looking down from above the solar north pole. Earth is the green circle to the right, and the positions of the two Solar Terrestrial Relations Observatory (STEREO) spacecraft (A, red circle; B, blue circle) are also shown; velocity is gauged by the color scale at top. Image at right shows a north-south cut along the Sun-Earth line. This model prediction proved to be a little early, with the main CME actually arriving at around 0100 UTC on 18 February

The ENLIL model:

Solves numerically the MHD equations in the inner heliosphere

$$
\begin{aligned}
\partial_t \rho + \nabla \cdot (\mathbf{v}\rho) &= 0 \\
\partial_t (\rho \mathbf{v}) + \nabla \cdot (\mathbf{v}\rho\mathbf{v} - \mathbf{B}\mathbf{B}) + \nabla p_{tot} &= 0 \\
\partial_t e + \nabla \cdot (\mathbf{v}e - \mathbf{B}\mathbf{B}\cdot\mathbf{v} + \mathbf{v}p_{tot}) &= \nabla \cdot (\mathbf{B} \times \eta\mathbf{J}) \\
\partial_t \mathbf{B} + \nabla \cdot (\mathbf{v}\mathbf{B} - \mathbf{B}\mathbf{v}) &= -\nabla \times (\eta\mathbf{J})
\end{aligned}
$$

$$
p = (\gamma - 1)(e - \rho\mathbf{v}^2/2 - \mathbf{B}^2/2) \quad p_{tot} = p + \mathbf{B}^2/2 \quad \mathbf{J} = \nabla \times \mathbf{B}
$$

Time dependent MHD model in spherical coordinate system + solves numerically the Differential Equations System.

Inner boundary conditions? → WSA model

The WSA model:

The model uses ground-based observations of the solar surface magnetic field as input to a magnetostatic potential-field source surface model to estimate the current sheet properties between 2.5 and 5 Rs.
Outward flows in the corona are approximated by the imposition of radial field boundary conditions at the source surface and by empirical relationships of expansion factors to initialize solar wind speeds at this point.
→ Solar wind driven by corotating background structure at its inner radial boundary at 21.5 Rs.

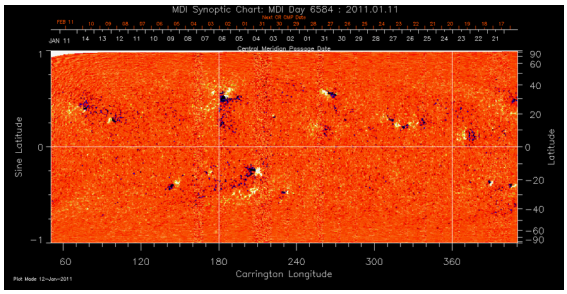

Illustration 13: HMI Carrington Rotation synoptic chart generated using near-central-meridian data from 20 magnetograms

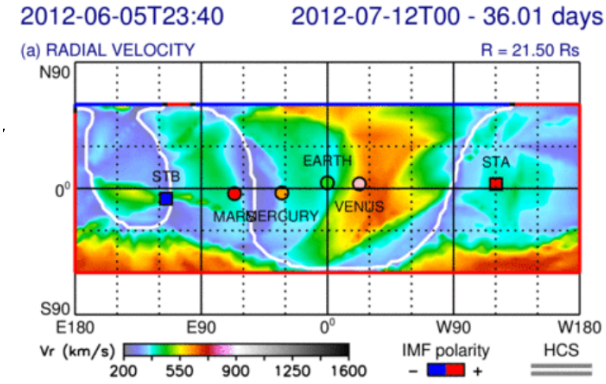

Illustration 12: WSA coronal maps generated from synoptic magnetograms

The combined WSA-ENLIL modeling provides specification of the solar wind flow speed, plasma density, solar wind mean plasma temperature, and magnetic field strength throughout the inner heliosphere.

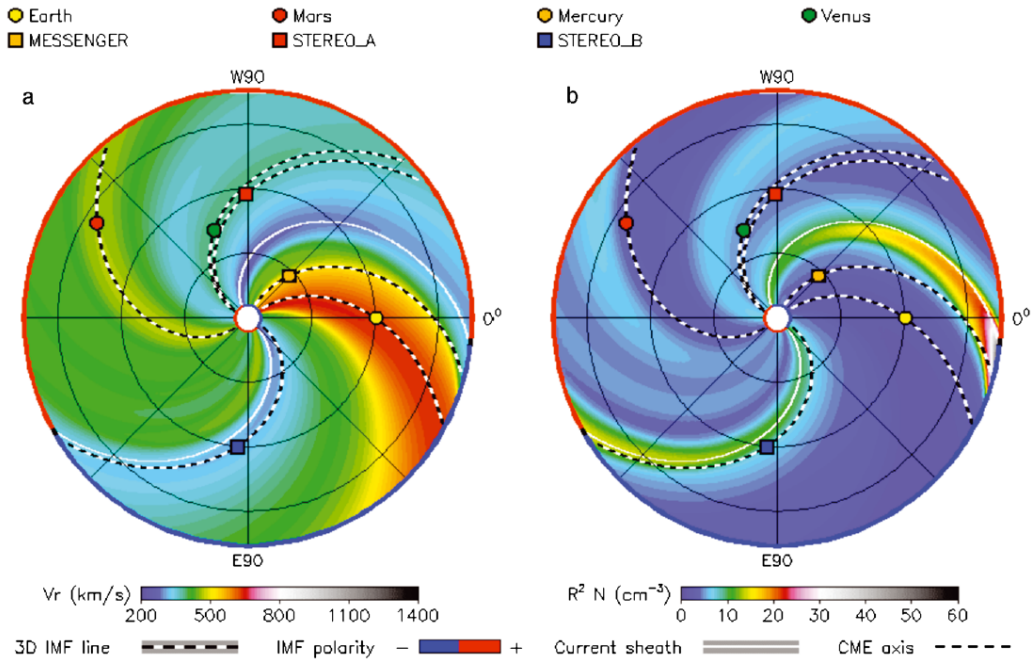

Illustration 14: Left: Modeled radial solar wind speed, viewed from the north ecliptic pole, obtained from theWSA-ENLIL model at an exemplary time when MESSENGER was in orbit around Mercury (3 May2011). The scale for Vr is given by the color bar. The locations of Earth, STEREO-A, STEREO-B, Venus,Mercury, Mars, and the MESSENGER spacecraft are indicated by small colored symbols. The inner domain of the model (where WSA is utilized) is denoted by the white central circle. The computational domain of the ENLIL simulation is shown by the colored area. The red-blue color coding along the edge of the outer boundary of computation shows the polarity of the IMF: red indicates IMF positive, or pointing away from the Sun, and blue indicates negative polarity with the IMF pointing toward the Sun. The white curves mark estimated IMF polarity sector boundaries near the equatorial plane. Right: WSA-ENLIL model results for density of the solar wind (normalized to 1 AU).

CME cone model

The CME input parameters at the ENLIL domain inner boundary are as follows,

1. Start date and time when the CME reaches the ENLIL inner boundary, i.e., 21.5 RS);
2. Cone latitude;
3. Cone longitude;
4. Cone half-width;
5. Take-off speed (km/s ; radial velocity at the ENLIL inner boundary).

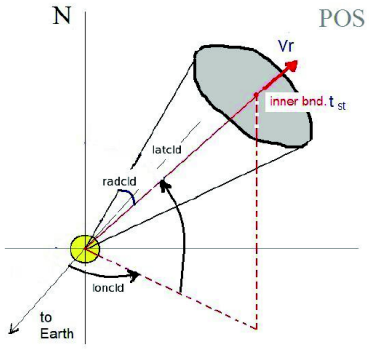

Illustration 15: Scheme for the Cone model for a CME

2 additional continuity equations for CMEs: density and polarity of the radial component of B

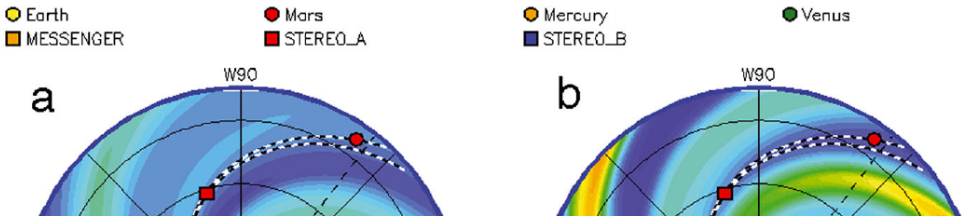

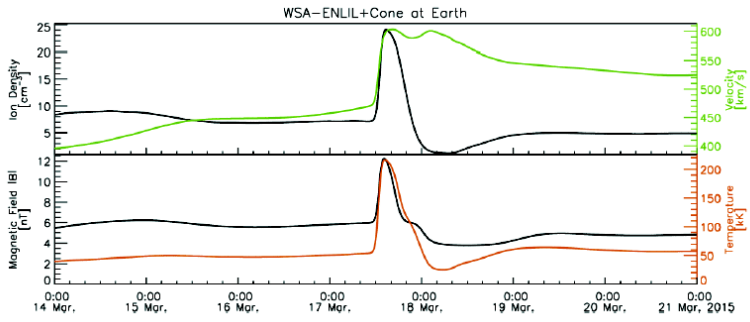

Illustration 17: Plot of the WSA-ENLIL+Cone model output quantities at 1AU.

EUHFORIA

A semi-empirical coronal model + heliosphere model including CMEs

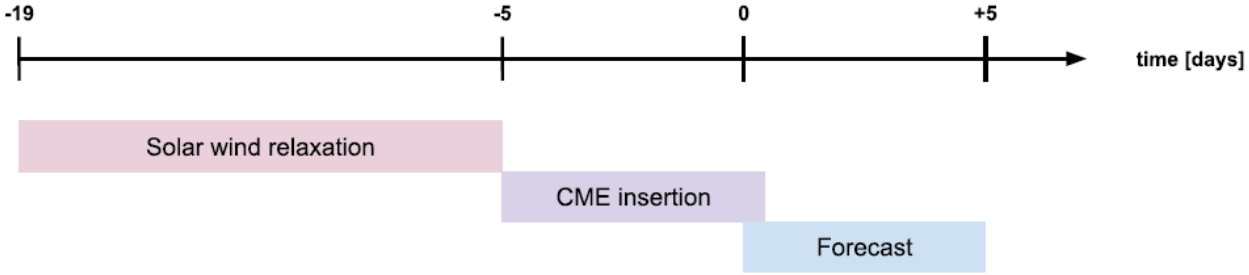

Illustration 18: The phases of the heliosphere simulation with typical durations. Each run starts with a solar wind relaxation, followed by a phase in which previously observed CMEs are introduced. The forecast starts is typically run for 5 days ahead.

solar wind plasma parameters at 0.1AU by a model of the coronal large-scale magnetic field and employing empirical relations to determine the plasma state (solar wind speed and mass density)

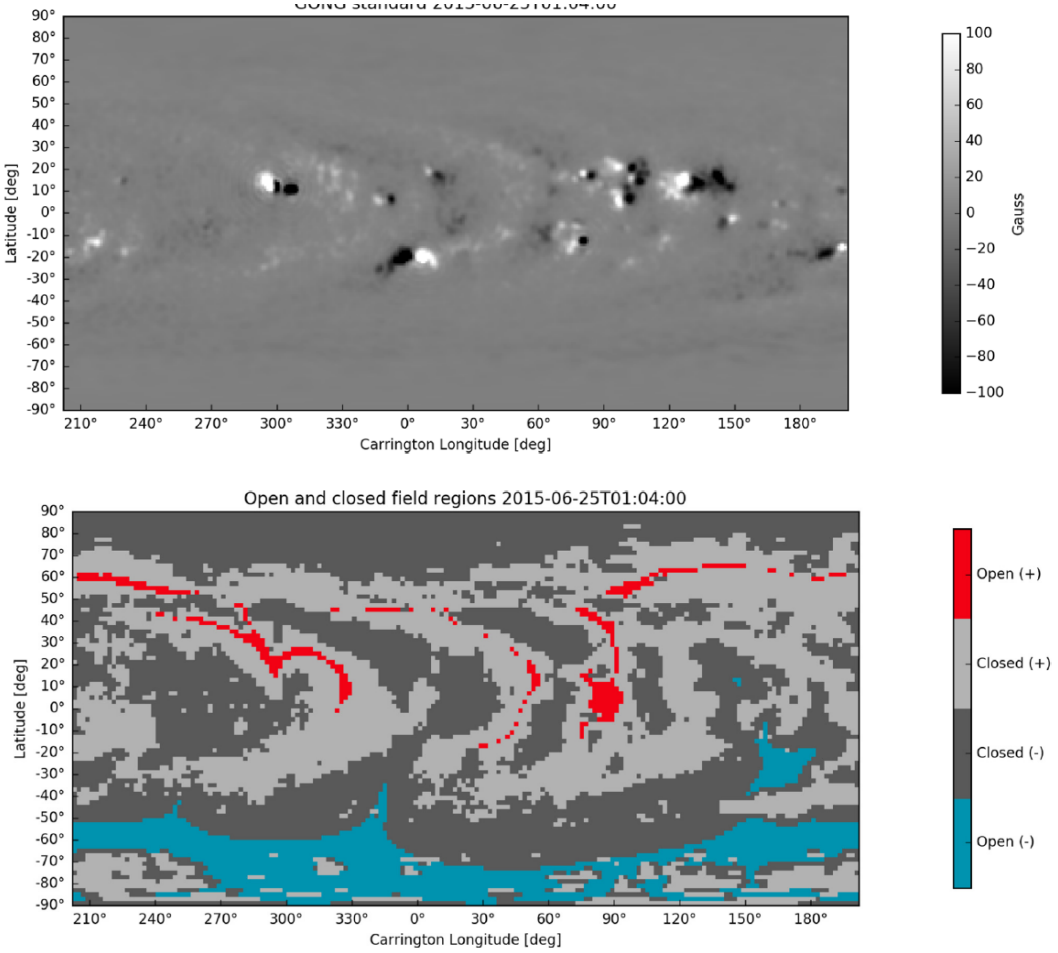

Illustration 19: Coronal magnetic field model. Top: Radial component of the magnetic field from data. Bottom: Open and closed B regions. Blue (red) pixels correspond to open field lines that continue in to the solar wind with a magnetic field pointing toward (away from) the Sun. Gray pixels indicate regions of closed magnetic topology.

The CMEs are introduced as a time-dependent boundary condition at the inner radial boundary at 0.1 AU
The parameters that the forecaster is required to supply for each CME are the mass density (rCME), temperature (TCME), velocity (vCME , uCME , fCME), angular width (vCME) and onset time at 0.1 AU.

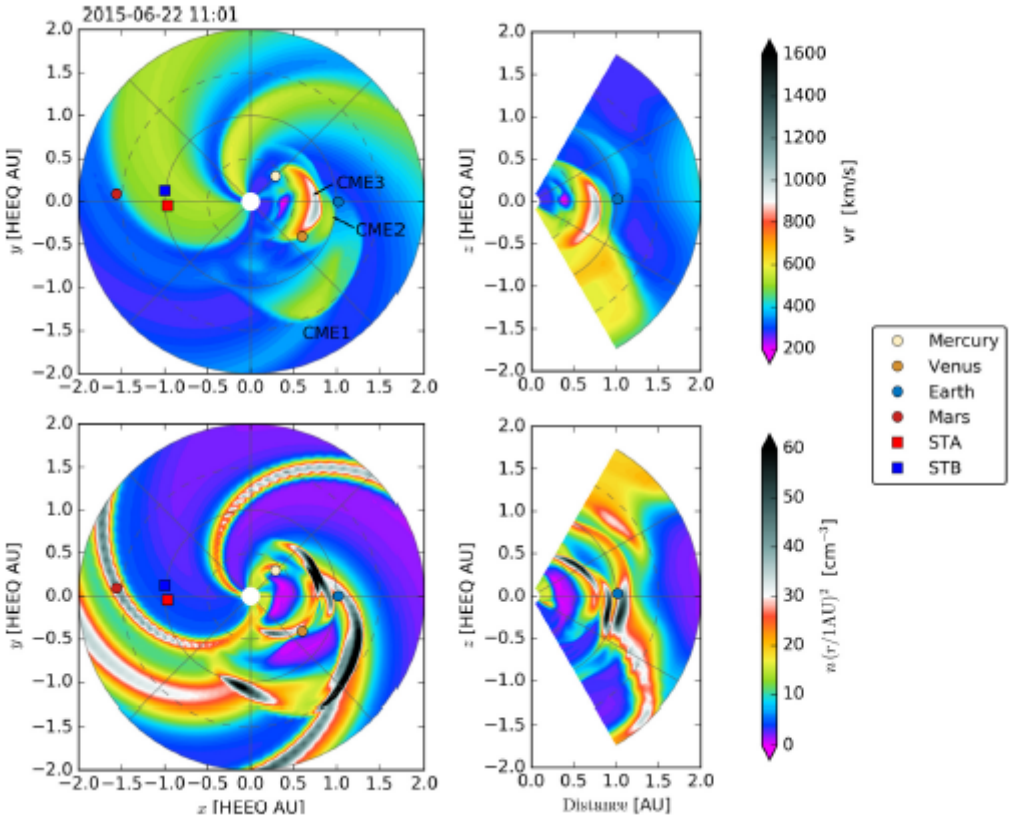

Illustration 20: Snapshot of the MHD simulation at 11:00 UT on June 22, 2015. Top row shows the radial speed, while the bottom row shows the scaled number density. The left panels depict the solution in the heliographic equatorial plane, while the right panels show the meridional plane that includes Earth.

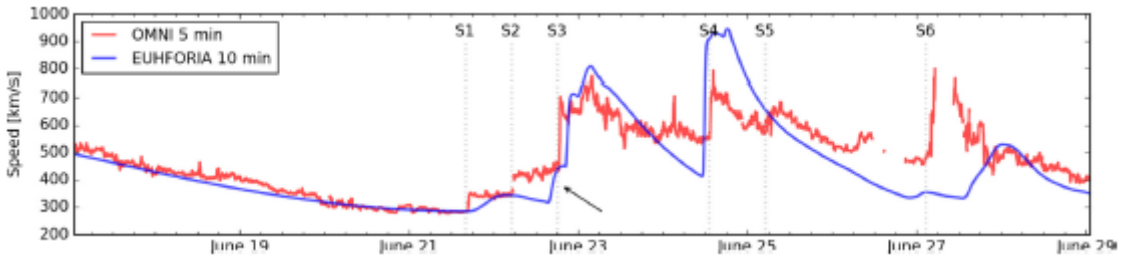

SUSANOO-CME

WSA model + Susanoo-SW + MHD CME

SUSANOO-SW to prepare the heliosphere inner boundary (r =30Rs)

CME internal magnetic field structure described with a distorted spheromak-type magnetic field

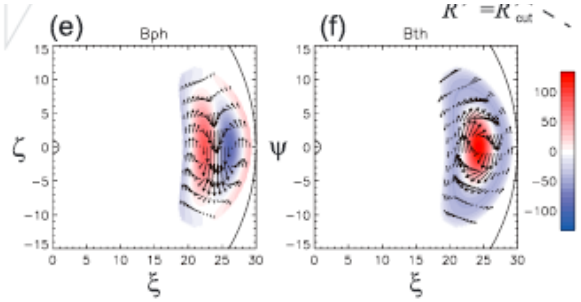

Illustration 22: Distribution of the magnetic field component normal to each plane in the spheromak CME model. The unit of the magnetic field isB0 = 8.864 nT.

List of parameters:

- Onset time of CME
- CME Propagation speed
- Heliographic latitude of CME source
- Heliographic longitude of CME source
- Tilt angle of spheromak
- Inclination angle of spheromak (0°)
- Chirality of helicity in spheromak (1/-1)
- Magnetic flux within CME (flare class)
- Angular width of CME (60°)
- Radial width of CME (2Rs)

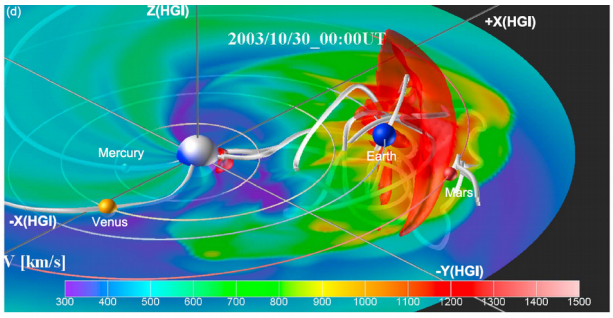

Illustration 23: Magnetic field structure. (a–c) Magnetic field structures on the meridional plane of the HEE coordinate where Earth is located. The color shows distribution of the toroidal component (By in HEE), and the arrows show magnetic field direction of poloidal component. (d) Three-dimensional view of CME 11 at the same timing as Figure 8b in HGI coordinate. The red surface shows high stream area whose speed exceeds 1200 km s−1. Background colors on the transparent XY plane in HGI (the solar equatorial plane) show solar wind velocity distribution. The thick tubes are magnetic field lines that connected around the positions of planets (shown with colored spheres associated with their orbits).

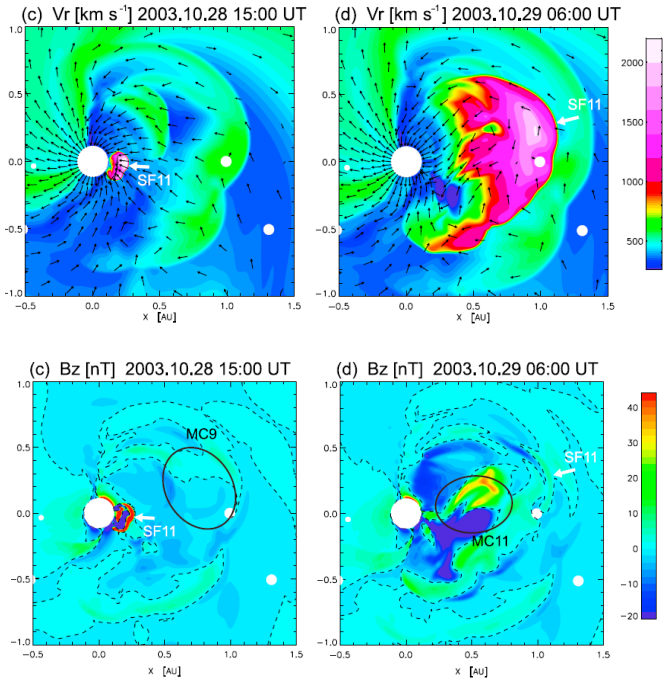

Illustration 24: Graphical output of a SUSANOO-CME simulation. The inner heliosphere is seen from above the ecliptic plane.

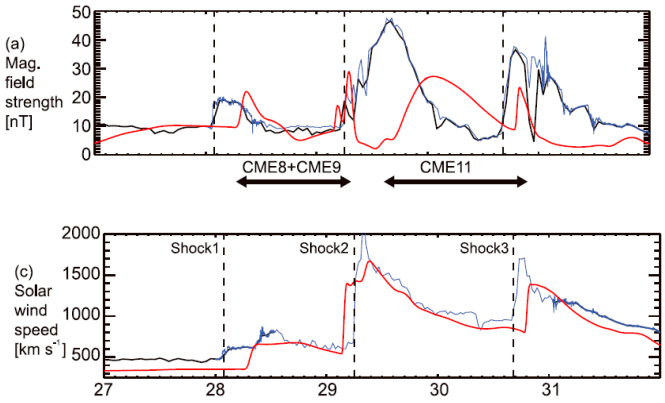

Illustration 25: Calculated (red line) and observed (black line and blue thin line) solar wind profiles at the Earth's position for 27–31 October 2003. The blue curves are ACE observations. The vertical dashed lines show the observed arrival times of three CME shocks.

DRAG BASED MODEL(s)

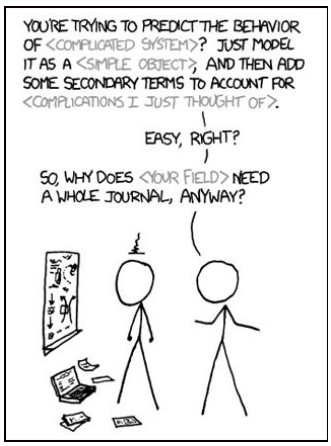

After the launch: >20 R_sun away

Negligible gravity + Negligible "acceleration" + Drag against environment (solar wind) + Self-similar expansion

$$F_d = -C_d A \rho (v - w)|v - w|,$$

$$r(t) = \pm \frac{1}{\gamma} \ln[1 \pm \gamma (v_0 - w)t] + wt + r_0,$$

The DBM needs four quantities, [r0 , v0 , w , g] to compute the heliospheric distance and velocity of the ICME at any t.

Shapes of CME:

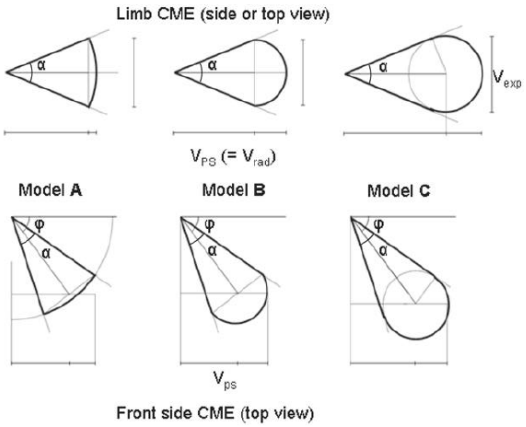

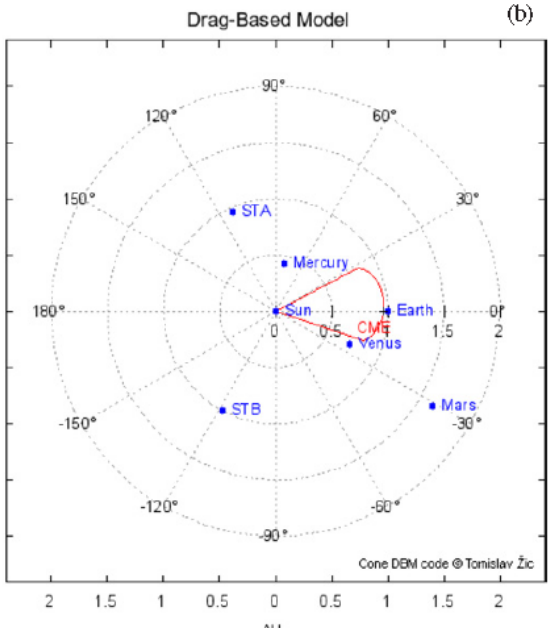

Illustration 26: The DBM simulation graphical output

Probabilistic/Ensemble approach:

PDBM and DBEM

N initial condition sets [r0, v0, γ, w] are randomly generated
N different [t@position, v@position] are computed

Obtain:
t_arrive ± t_error
v_arrive ± v_error

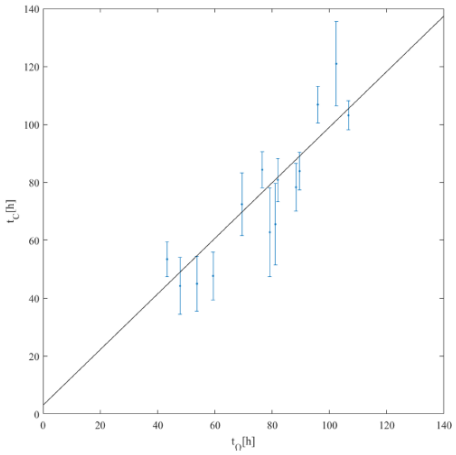

Illustration 28: Dots with error bars are the PDBM forecast transit times versus observed transit times. The solid line shows a linear fit to the data.

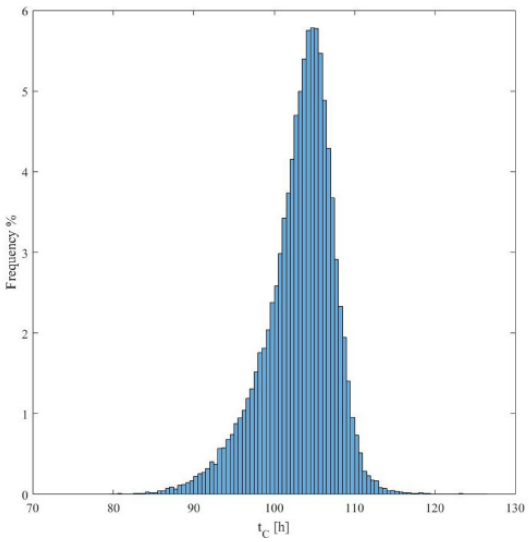

Illustration 27: Distribution of the transit times calculated for the 12 Dec 2008 CME. N = 50000 initial conditions are generated in the P-DBM

Which information do we have to feed the models?

a) Solar Wind
- Speed
- Direction
- Associated B

b) CME parameters

• Onset time	Δt=0-2 hours
• Source	ΔΦ=>5°
• Speed	Δv=10-1000 km/s
• Direction	ΔΘ=~10°
• Associated B	ΔB=?

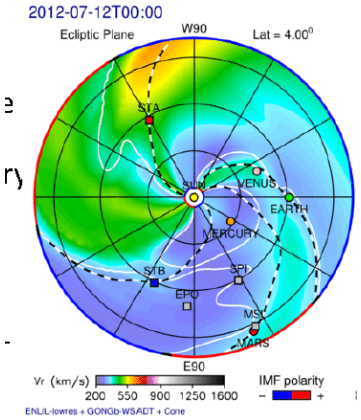

Illustration 29: Initial solar wind model for a WSA-ENLIL+Cone forecast

Both a) and b) have
(large) errors and unknowns.

...and things will get worse in the future!

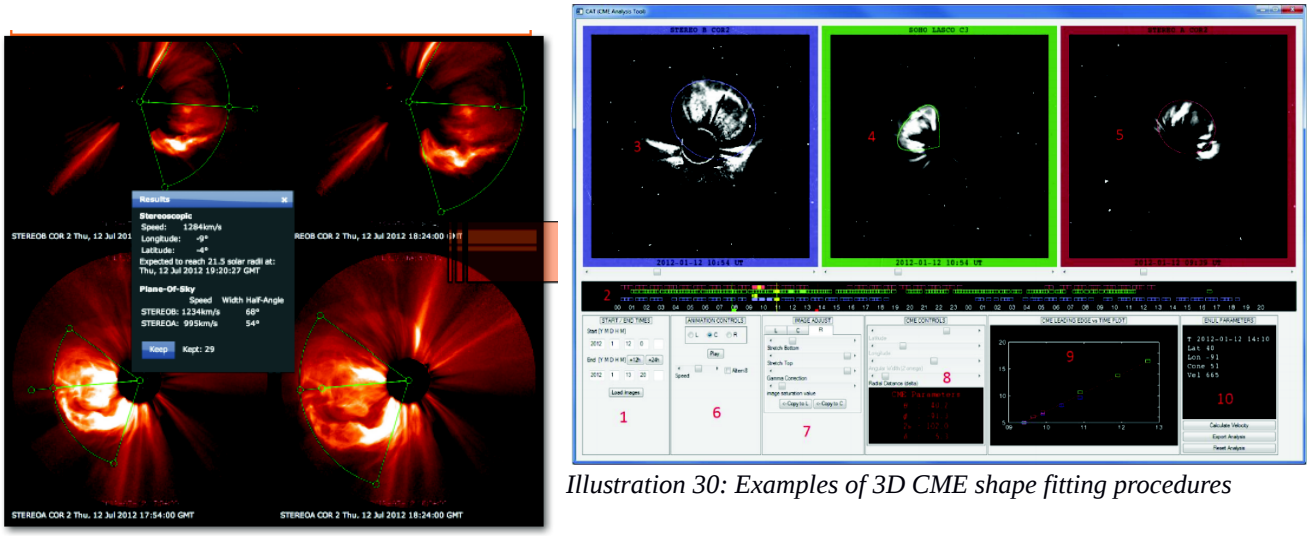

Illustration 30: Examples of 3D CME shape fitting procedures

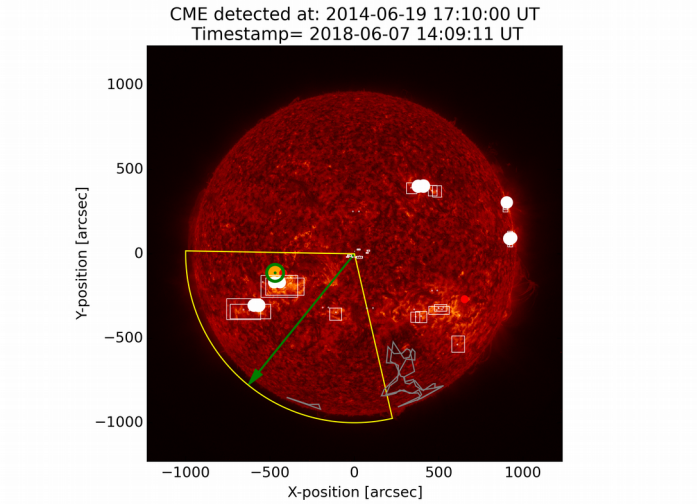

*Illustration 31: Example of graphical output of an automated CME **source** finding procedure*

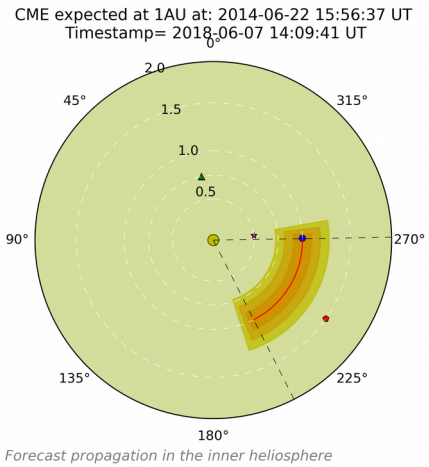

*Illustration 32: Example of graphical output of an automated CME **propagation** model*

How well do we forecast?

CCMC scoreboard!
a research-based CME forecasting methods validation activity
https://kauai.ccmc.gsfc.nasa.gov/CMEscoreboard/
Note: the performance of the <u>average of the various models forecasts</u> is <u>better</u> than the performance of <u>any of the models</u>!

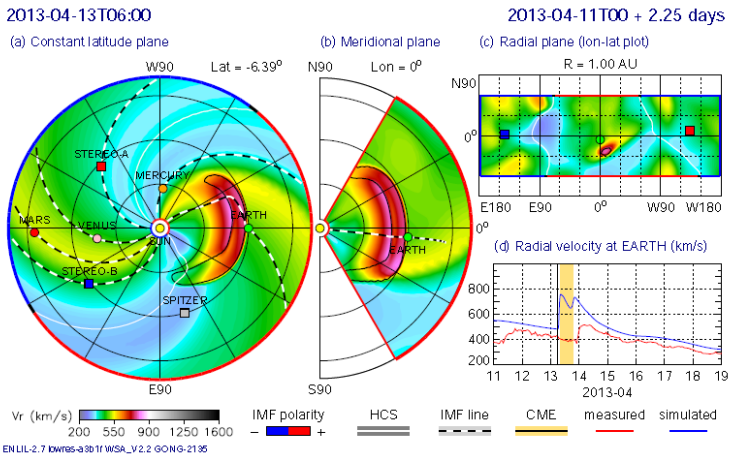

Illustration 34: Global view of 11 April 2013 CME on 13 April at 06:00 UT: median CME of the ensemble

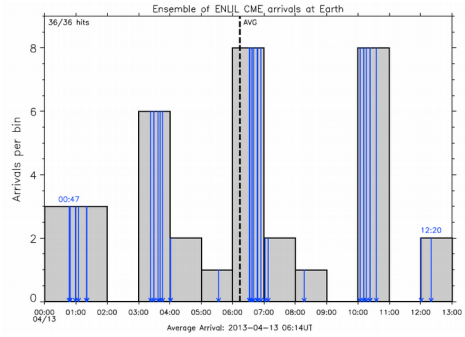

Illustration 33: 11 April 2013 base ensemble: Histogram of distribution of arrival time predictions at Earth (one hour bin size). The actual arrival was observed on 13 April at around 22:13 UT by Wind.

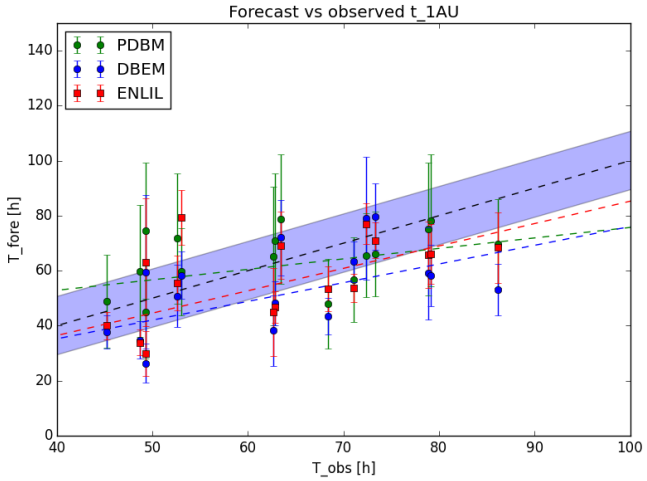

Illustration 36: Computed vs observed transit time for different CME propagation models. Colored dashed lines are best fit. The black dashed line represents the perfect match. The blue shadowed area represent the expected dispersion form the perfect match.

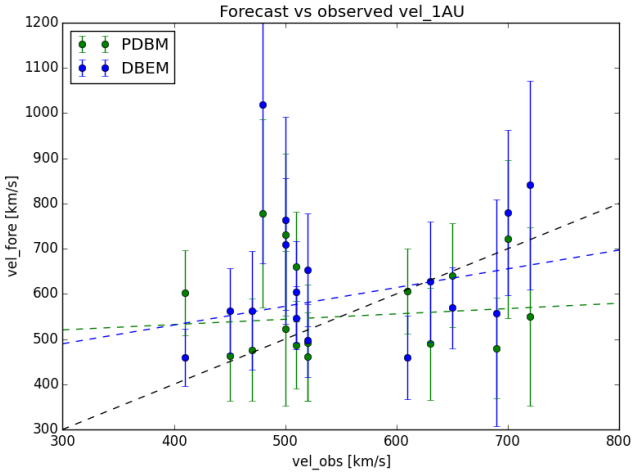

Illustration 35: Computed vs observed velocity at 1AU for different CME propagation models. Colored dashed lines are best fit. The black dashed line represents the perfect match.

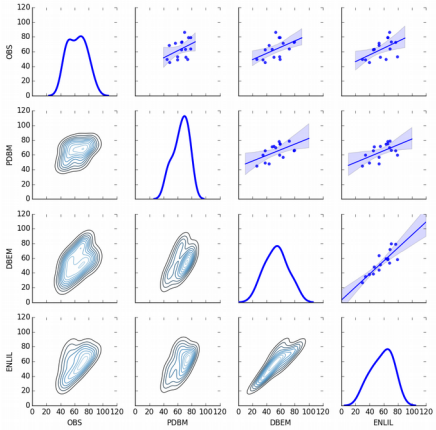

Illustration 37: Correlations and regressions for observation and models against each other.

Want to know more?

CME facts:

Gopalswamy, N., L. Barbieri, E. W. Cliver, G. Lu, S. P. Plunkett, and R. M. Skoug (2005), **Introduction to violent Sun-Earth connection events of October–November 2003**, J. Geophys. Res., 110, A09S00, doi:10.1029/2005JA011268.

Forbes, T.G., Linker, J.A., Chen, J. et al. **CME Theory and Models**, Space Sci Rev (2006) 123: 251. https://doi.org/10.1007/s11214-006-9019-8

P.F. Chen **Coronal mass ejections: models and their observational basis** Living Rev. Sol. Phys., 8 (2011)

Webb, D.F., and T.A. Howard, **Coronal mass ejections: observations**, Living Rev. Sol. Phys., 9, 3, 2012.

WSA-ENLIL+Cone model:

Arge, C.N., Pizzo, V.J.: 2000, I**mprovement in the prediction of solar wind conditions using near-real time solar magnetic field updates**. J. Geophys. Res. 105, 10465 – 10480. doi:10.1029/1999JA000262.

Odstrcil, D.: 2003, **Modeling 3-D solar wind structure**. Advances in Space Research 32, 497 – 506. doi:10.1016/S0273-1177(03)00332-6.

Odstrcil, D., Pizzo, V.J.: 1999a, **Three-dimensional propagation of CMEs in a structured solar wind flow: 1. CME launched within the streamer belt**. J. Geophys. Res. 104, 483 – 492. doi:10.1029/1998JA900019.

Odstrcil, D., Pizzo, V.J.: 1999b, **Three-dimensional propagation of coronal mass ejections in a structured solar wind flow 2. CME launched adjacent to the streamer belt**. J. Geophys. Res. 104, 493 – 504. doi:10.1029/1998JA900038.

Odstrcil, D., Riley, P., Zhao, X.P.: 2004, **Numerical simulation of the 12 May 1997 interplanetary CME event**. J. Geophys. Res. 109, 2116. doi:10.1029/2003JA010135.

Xie, H., Ofman, L., Lawrence, G.: 2004, **Cone model for halo CMEs: Application to space weather forecasting**. J. Geophys. Res. 109, 3109. doi:10.1029/2003JA010226.

Mays, M. L., et al. (2015), **Ensemble modeling of CMEs using the WSA-ENLIL+Cone Model**, Sol. Phys., 290, 1775–1814, doi:10.1007/s11207-015-0692-1.

EUHFORIA:

Pomoell J, Poedts S (2018) **EUHFORIA: EUropean Heliospheric FORecasting Information Asset**. J Space Weather Space Clim 8:A35. https://doi.org/10.1051/swsc/2018020

SUSANOO-CME:

Kataoka, R., T. Ebisuzaki, K. Kusano, D. Shiota, S. Inoue, T. T. Yamamoto, and M. Tokumaru (2009), **Three-dimensional MHD modeling of the solar wind structures associated with 13 December 2006 coronal mass ejection**, J. Geophys. Res., 114, A10102, doi:10.1029/2009JA014167.

Shiota, D., R. Kataoka, Y. Miyoshi, T. Hara, C. Tao, K. Masunaga, Y. Futaana, and N. Terada (2014), **Inner heliosphere MHD modeling system applicable to space weather forecasting for the other planets**, Space Weather, 12, 187–204, doi:10.1002/2013SW000989.

Shiota, D., and R. Kataoka, **Magnetohydrodynamic simulation of interplanetary propagation of multiple coronal mass ejections with internal magnetic flux rope (SUSANOO-CME)**,(2016) Space Weather, 14, 56–75, doi:10.1002/2015SW001308.

BDM and sons:

Vrsnak, B., et al., 2013. **Propagation of interplanetary coronal mass ejections: the drag based model**. Sol. Phys. 285, 295–315. http://dx.doi.org/10.1007/s11207-012-0035-4.

Vršnak, B., et al., 2014, **Heliospheric Propagation of Coronal Mass Ejections: Comparison of Numerical WSA-ENLIL+Cone Model and Analytical Drag-based Model**. Astrophys. J. Supp. 213, 21. doi:10.1088/0067-0049/213/2/21.

Dumbović, M.; Čalogović, J.; Vršnak, B.; Temmer, M.; Mays, M. L.; Veronig, A.; Piantschitsch, I. (2018), "**The Drag-based Ensemble Model (DBEM) for Coronal Mass Ejection Propagation**", ApJ, 854, 180. doi:10.3847/1538-4357/aaaa66

Napoletano, G.; Forte, R.; Del Moro, D.; Pietropaolo, E.; Giovannelli, L.; Berrilli, F. (2018), "**A probabilistic approach to the drag-based model**", J. Space Weather Space Clim. 8 A11. doi: 10.1051/swsc/2018003

OTHERS:

Manchester, W. B., et al. (2004), **Three-dimensional MHD simulation of a flux rope driven CME**, J. Geophys. Res., 109, A01102, doi:10.1029/2002JA009672.

Manchester, W. B., et al. (2004), **Modeling a space weather event from the Sun to the Earth: CME generation and interplanetary propagation**, J. Geophys. Res., 109, A02107, doi:10.1029/2003JA010150.

Manchester, W. B., B. van der Holst, and B. Lavraud (2014), **Flux rope evolution in interplanetary coronal mass ejections: The 13 May 2005 event**, Plasma Phys. Controlled Fusion, 56(6), 064006, doi:10.1088/0741-3335/56/6/064006.

Paouris, E. and Mavromichalaki, H. **Effective Acceleration Model for the Arrival Time of Interplanetary Shocks driven by Coronal Mass Ejections,** Sol Phys (2017) 292: 30. doi:10.1007/s11207-017-1050-2.

A.P. Rouillard, et al. **A propagation tool to connect remote-sensing observations with in-situ measurements of heliospheric structures** Planet. Space Sci. (2017) 147, 61 doi.org/10.1016/j.pss.2017.07.00